Granular Matter (2026) 28:35
https://doi.org/10.1007/s10035-025-01597-6

RESEARCH

Robot excavation and manipulation of geometrically cohesive granular media

Laura K. Treers[1] · Daniel Soto[2] · Joonha Hwang[3] · Michael A. D. Goodisman[4] · Daniel I. Goldman[2]

Received: 26 July 2025 / Accepted: 30 October 2025

Abstract
Robots capable of manipulating cohesive materials would be beneficial in a variety of complex construction tasks. To discover principles by which robotic systems can effectively manipulate entangled granular media, we develop a robophysical platform for interaction with media composed of u-shaped particles. This robotic platform uses environmental signals to autonomously coordinate excavation, transport, and deposition of material. We test the effect of material initial conditions by characterizing robot performance in two different material compaction states, and observe as much as a 75% change in transported mass depending on initial material compressive loading. This large difference suggests the functional role that properties such as packing and geometric cohesion play in excavation and manipulation. To better understand these properties, we develop an apparatus for tensile testing of the geometrically cohesive media, which reveals how entangled material strength depends strongly on initial compressive loading. These results rationalize the variation observed in robotic performance and point to future directions for better understanding robotic interaction with entangled materials.

Keywords Geometrically entangled media · Manipulation · Robophysics

1 Introduction

There is increasing interest in developing robotic teams for collective construction [1]. Such robot teams have many potential applications, from the construction industry to disaster response to space exploration. Existing experimental mobile robotic systems have largely drawn from concepts more typical in conventional construction, utilizing building elements such as rigid bricks, struts, or blocks [2, 3]. Some recent work has explored the use of amorphous materials such as foams [4, 5] concrete [6], or on-site materials such as pebbles [7–9]. Some researchers have also developed tools for robotic manipulation of granular media through perception [10] or learning [11, 12].

A recent approach for construction embraces disorder in the configuration of the building elements, and therefore may be particularly well-suited for construction using mobile robots. This approach, termed aleatory architecture, suggests that structural stability can emerge via particle jamming, rather than through precise placement of the building elements [13, 14]. In turn, aleatory structures can be "self-healing," and can be built in environments where utilizing predetermined blueprints and construction materials is impossible. Architects and designers have explored this new

Laura Treers and Daniel Soto contributed equally to this work.

✉ Daniel I. Goldman
daniel.goldman@physics.gatech.edu

Laura K. Treers
laura.treers@uvm.edu

Daniel Soto
dsoto7@gatech.edu

Joonha Hwang
jhwang321@gatech.edu

Michael A. D. Goodisman
michael.goodisman@biology.gatech.edu

[1] Department of Mechanical Engineering, University of Vermont, 33 Colchester Ave., Burlington, VT 05405, USA

[2] School of Physics, Georgia Institute of Technology, 837 State St., Atlanta, GA 30332, USA

[3] George W. Woodruff School of Mechanical Engineering, Georgia Institute of Technology, 801 Ferst Dr NW, Atlanta, GA 30318, USA

[4] School of Biological Sciences, Georgia Institute of Technology, 310 Ferst Dr. NW, Atlanta, GA 30332, USA

Published online: 27 February 2026

design paradigm in recent years, and have demonstrated that a variety of particle shapes and sizes can be utilized for creating rigid structures with little preplanning [15, 16].

Many aleatory structures that have been created thus far have relied on pouring or forming particles into molds [14] (Fig. 1A). Thus, these structures have often relied on human intervention for their creation. In contrast, robotic fabrication of aleatory structures remains a nascent research area [15]. Some recent works have explored the use of cable-driven parallel robots for in-situ construction with non-convex particles [17]; groups of fixed six-axis robotic arms for depositing granular aggregate and tensile elements to create jammed structures [18]; as well as a singular robotic arm on a mobile platform for laying rock and string into aleatory column structures [19].

We hypothesize that aleatory systems are well-suited for distributed collective construction by mobile robotic platforms (Fig. 1B): in particular, geometrically entangled materials are able to provide strong cohesive forces without the requirement for adhesives or interstitial fluid [20–23], making them suitable for repeatable manipulation and transport. Geometrically entangled materials generate an effective cohesion at the macroscopic level via their particles' concave shape, as opposed to chemical cohesion at the microscopic level. We refer to such groups of interpenetrating particles as entangled "ensembles." Additionally, because these entangled materials do not rely on interstitial fluid to provide cohesive forces, their material properties can be well-characterized in the laboratory setting.

Prior work has shown that longer entangled ensembles are weaker than shorter ones [24], and that ensemble strength is sensitive to particle geometric properties [22, 25]. More recent work has also explored their extensional rheology, demonstrating stick–slip behavior during tension caused by local yielding and rearrangement of particle entanglements [24–26]. Still, many questions remain unanswered with regard to the behavior of these materials, including their response to external loading. Some recent work has demonstrated a stress-induced anisotropy [27], as well as compression and shear-driven jamming behavior [28]. Better understanding these non-traditional material behaviors in an experimental setting will be important for developing strategies for material manipulation and transport.

The manipulation of cohesive materials represents a particularly challenging task, as it requires tearing or separating some subset of particles from a larger entangled ensemble, and subsequent (or simultaneous) re-forming or consolidation of that subset of particles for transport and/or deposition. Because of the complex nature of these interaction mechanics, the principles by which geometrically cohesive materials need to be manipulated, and by which they can then be utilized to form structures, remain unknown. For example, which types of manipulation strategies result in successful separation of material? Similarly, what are effective methods for re-strengthening cohesive materials once separated? And lastly, how should agents decide if and where to begin excavating materials?

In this work, we develop strategies for robust manipulation of geometrically cohesive materials. We do so by building a robophysical platform [29] capable of autonomously excavating and transporting geometrically cohesive media. We study trends in excavation performance during autonomous operation for various material preparation states. We then seek to understand the robotic performance trends and test strategies for material manipulation via material tensile testing, and demonstrate a strong correlation between external loads and subsequent tensile strength in entangled materials. The results from this robophysical study have implications for the future design of individual robot manipulation strategies, as well as for the future deployment of robotic teams.

2 Robophysical platform for interaction with cohesive media

2.1 Methods: design of robophysical platform and testing environment

Our robotic agent for manipulating cohesive granular media is a 3D-printed modified minimal locomotor design (length and width = 32 cm, height = 18 cm) (Fig. 2). The robotic agent has five Dynamixel AX12A motors: two 2-DoF front limbs equipped with 3D-printed nylon "claws" and one motor driving a pair of rear 3D-printed "whegs" [30] that are equipped with rubber treads for traction. An external

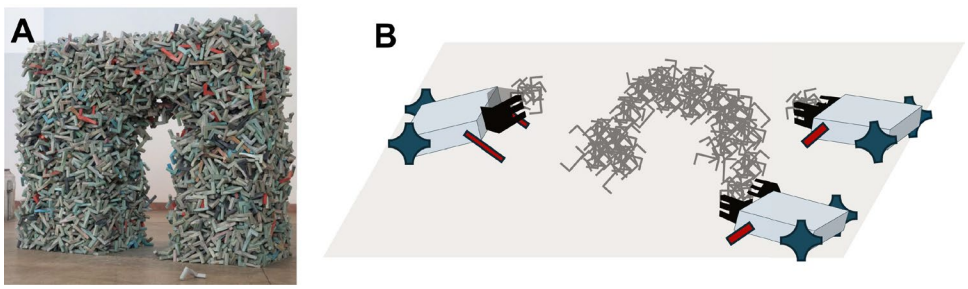

Fig. 1 Aleatory architectures and robotic construction. **A** Example of an aleatory structure realized through geometrically entangled Z-shaped particles, each 14 cm along their length. Adapted from [14]. **B** Concept for robot teams building aleatory structures

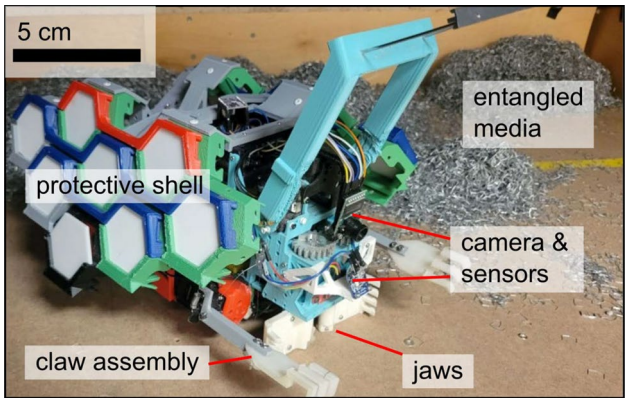

Fig. 2 Image of the robophysical platform used in this work. We use this robotic agent to study the manipulation and transport of geometrically cohesive granular material, which can be used to inform future engineering design. The entangled material, robot jaws and claws used for material manipulation, as well as the sensors and cameras used for navigation, and protective shell are labeled

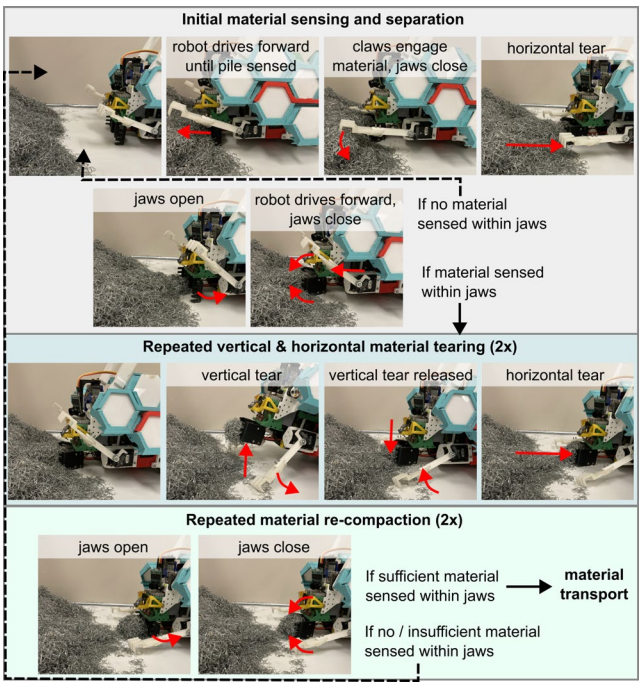

Fig. 3 Illustrations of robot excavation strategies. Depiction of excavation sequence, including grasping and tearing of geometrically entangled media

shell comprised of hexagonal plates protects internal electronics from particle ingress. The robot is battery powered and utilizes a suite of sensors for navigation and material sensing, which are described in Appendix A .

We use u-shaped particles (office staples) as geometrically entangled media in this work [22]. Each particle has a length of 12 mm along its longest axis and two perpendicular segments of length 6 mm. We detached approximately 500,000 staples from one another using acetone to dissolve the binding adhesive. The resulting material is capable of forming amorphous 3D load-bearing structures without the need for chemical or capillary cohesion.

The robot operates within a constructed "arena" and uses lights to coordinate movement between an "excavation zone" and "deposition zone". The details of this arena setup are described in Appendix B. The robotic agent's microcontroller executes a finite state machine (FSM) based on the testing environment described above (a full description of the FSM is provided in Appendix C). The FSM embodies the different behaviors needed for the robotic agent to excavate material, transport it to the deposition site, and finally return to the excavation site to repeat the process. The robot transports small mounds of entangled particles, which we term "pellets." The transitions between behaviors are governed by environmental signals in the form of fixed light sources and object proximity information, which are detected via onboard sensors. The deposition process involves a search algorithm to find existing piles on which to deposit pellets, with the goal of creating emergent structures from cohesive material; this search process is also described in Appendix C. However, in this work, we focus specifically on the mechanics of interaction required to tear and separate material during the excavation process.

2.2 Results and discussion

2.2.1 Excavation and material manipulation strategy

The robot manipulates geometrically cohesive material using a set of interlocking jaws, which allow the robot to penetrate and engage small regions of a staple ensemble (Fig. 3). These jaws are 3D printed and are actuated by a single Dynamixel AX12A motor. The process of removing pellets of material from a larger mound requires repeated large stressing events, or application of large tensile forces, which are stronger than what the jaws alone could provide. In order to successfully separate pellets from the larger ensemble, we implement an excavation procedure, illustrated in Fig. 3. We discover that a sequence of initial material sensing and horizontal separation, followed by repeated vertical and horizontal tearing (using the limbs and rear whegs, respectively), enables material separation. By engaging the limbs during the excavation procedure, the robot effectively weakens the connection between the pellet within the jaws and the rest of the mound, thus allowing the robot to remove a subset of material and transport it elsewhere.

Lastly, we observe that separation alone through tearing is not sufficient for material transport. As a result of the excavation process, the separated material is often less cohesive, leading to dropping of individual particles during transport. To address this concern, we introduce a final step

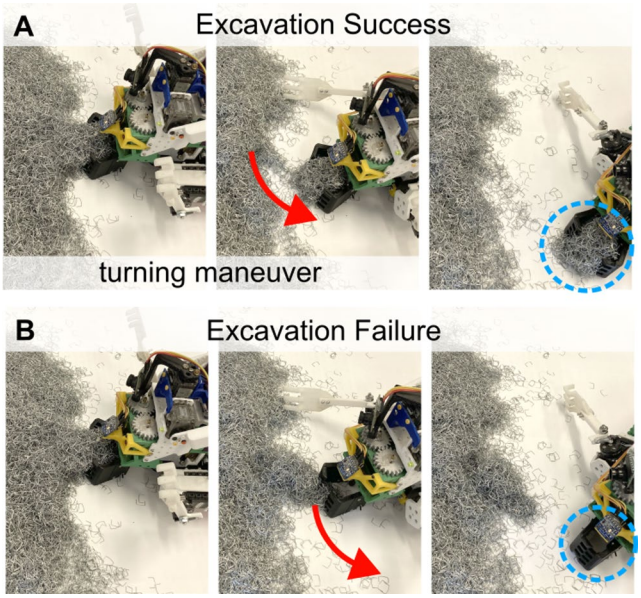

Fig. 4 Depiction of robot excavation performance. **A** Robot excavation success, in which a pellet of material is formed and transported. **B** Excavation failure, in which the material excavated is either dropped or not separated from the larger ensemble

to the excavation procedure which repeatedly re-compacts the separated material using the jaws, creating a cohesive pellet that can then be transported. The number of cycles needed to remove the pellet from the mound varies with the size of the pellet, the material packing state, and the local topology of the mound. Given that these conditions are highly variable and can change over time, the robot does not perform a fixed number of excavation procedures. Instead, the robot runs this protocol until the jaws are unable to fully close after the robot has backed away from the mound. This condition is measured using the Dynamixel motor's internal encoders, which indicate whether the jaw angle is greater than a threshold of $\approx 30^o$. This state signifies that material is in the jaws and that the robot has successfully removed a "pellet" from the mound.

2.2.2 Evaluation of performance

We evaluate the performance of the robot excavating and transporting material with three metrics: average cycle time, excavation success rate, and total material transported. The first two metrics are computed through manual video parsing. Within each cycle, excavation success is determined through the oblique camera: if the agent breaks off material from the excavation pile and retains at least one quarter of the jaws' capacity (≈ 3 cm^3) by the end of its turning maneuver, it is marked as an excavation success (Figure 4A). Once a trial is complete, we gather the material at the deposition site and weigh it, providing a final performance metric. These methods quantify robot performance across trials and help characterize the challenges associated with cohesive material manipulation.

2.2.3 Excavation performance

We first characterize the robot's performance to understand which strategies result in successful material manipulation. In an initial set of experiments, we replicate trials with repeatable material characteristics to identify both successful material transport as well as failure modes. We prepare the arena such that piles of staples are shaken from $\approx$ 0.3 m above the arena floor, ensuring that individual staples or very small groups fall within a fixed rectangular region (1.2 $\times$ 0.3 m) adjacent to the wall. Over two hours, the robot performs cycles of excavation and deposition (Fig. 5A). As shown in Fig. 5B, the number of pellets excavated grows approximately linearly in all five trials tested. However, late in the trials, we observe the emergence of a failure mode in the excavation process: when the robot has completed multiple cycles of tearing, backs away from the pile, and still senses material within its jaws, the algorithm infers that material has been separated and the robot switches to transport. However, depending on the relative strength of the staple ensemble, the material within the jaws may be "stretched" but still attached to the main ensemble via strong tensile forces.Thus, in these scenarios, the robot is unable to

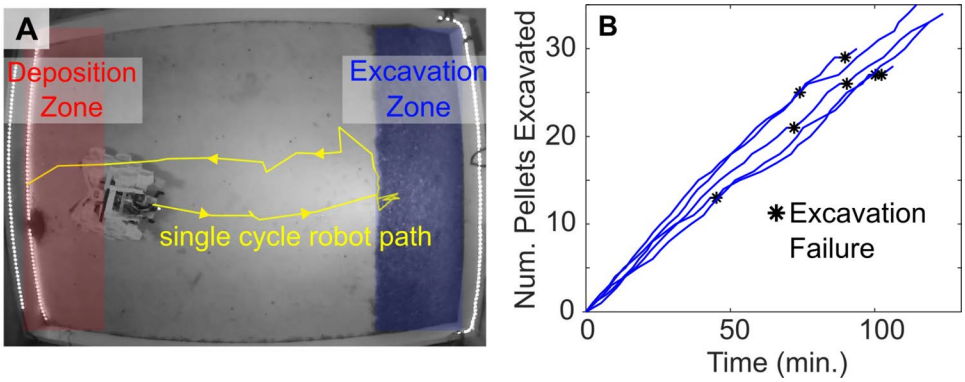

Fig. 5 Robotic excavation and deposition cycles. **A** Depiction of robot path in its testing environment, during a cycle of excavation and deposition. **B** Number of pellets excavated over time for five trials. Asterisks indicate excavation failures

separate the material within its jaws for transport. Eventually, the material slips out of the jaws during the attempts to turn, and we denote these instances as excavation failures, as shown in Fig. 4B (denoted with asterisks in Fig. 5B).

Because we observe most excavation failures occur late in the trials, we hypothesize that repeated cycles of excavation may disturb and compress the material over time, leading to a relative strengthening via entanglement of particles. The robot is only able to sense the volume of material it has grasped, and not the force required to tear away that material. As a result, the robot is unable to respond to changes in material tensile strength over time. Thus, we hypothesize excavation failures are more likely to occur later in the trial, when the material has higher tensile strength. These results suggest the possibility of a compression-dependent strengthening of entangled media, which we explore via controlled variation in material properties.

2.2.4 Effect of material properties on robot behavior

We next test our prior hypotheses and further investigate how material properties impact the excavation process. We conduct two sets of experiments in which we prepare the material at the excavation site in one of two methods: "scattering" and "pushing."

In the "scattering" preparation mode, identical to the prior section, piles of staples are shaken such that individual

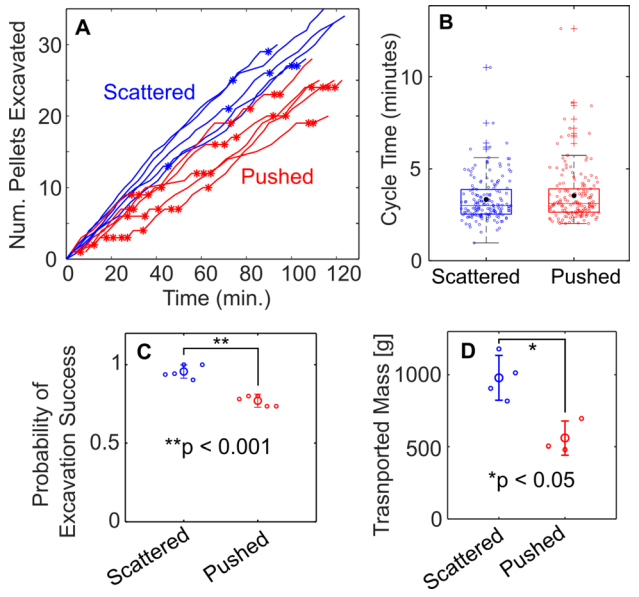

Fig. 6 Pellet excavation performance for two material preparation states. **A** Number of pellets excavated over time for five trials of each tested material condition. Asterisks indicate excavation failures. **B** Cycle times for all trials, compared between scattered and pushed material states. Plus signs indicate outliers. **C** Comparison in mean excavation success over two hours between scattered and pushed material states. **D** Comparison of total transported mass of material at the end of trials for both scattered and pushed states

particles fall within the fixed region adjacent to the arena wall. In the "pushing" mode, the same number of staples are instead scattered across the entire arena area, and then are pushed to be contained within the same rectangular region. The volume fractions of portions of staples from each of these preparations were 0.072 ± 0.005 and 0.117 ± 0.002 for pushing and scattering, respectively. Notably, pushed conditions have fewer staples per unit cell than the scattered case. We hypothesize that the disturbances which occur during pushing alter the media strength, and thus these two preparation modes probe the sensitivity of manipulation performance to material characteristics.

After five trials of approximately two hours for both the scattered and pushed material states, we analyze the proportion of successful excavation over two hours as a function of the initial material states. The robotic agent has limited sensing capabilities and there is wide variability in material states; as a result, the robot does not successfully remove material each time it exits the excavation area. Thus, we denote whether material is successfully removed at every cycle, and observe that more pellets are excavated successfully over time in the scattered condition (Fig. 6A). In turn, we find that the excavation probability is dependent on initial material preparation (Fig. 6C). In the scattered condition, the robot successfully removes material with a probability of 0.96 ± 0.04, whereas in the pushed initial condition, this likelihood decreases to 0.77 ± 0.03. We observe statistical significance in excavation success between conditions with $p = 0.00054$. Despite these differences in excavation probabilities, we see little statistical difference between the distributions of cycle times for each initial material state (Fig. 6B), with scattered and pushed cycles taking 3.3 ± 1.2 and 3.5 ± 1.5 min, respectively.

We observe 75% more mass transported in the scattered condition than the pushed condition (Fig. 6D); however, this discrepancy in performance is not reflected by the difference in excavation success. Instead, we observe a 25% higher excavation success rate in the scattered condition than the pushed condition. This discrepancy could be explained by differences in transported pellet size and mass, or differences in relative density of the transported material between these two states.

In summary, these results demonstrate that robot manipulation performance is highly sensitive to material properties. Further, we hypothesize that the significant discrepancies in performance may be attributed to variation in material strength between the two preparation states. In the "pushed" preparation mode, compression or other disturbance to the media may lead to different material behavior than in the "scattered" case, resulting in wide variation in excavation performance. We further investigated this dependence

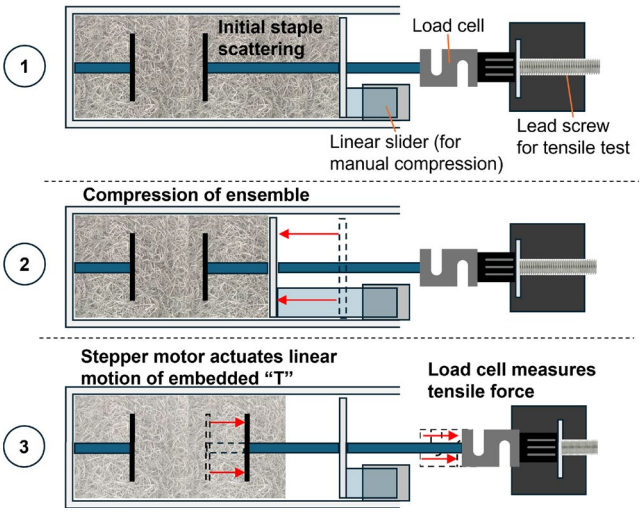

Fig. 7 Diagram of staple testing apparatus. **(1)** Staples are initially scattered in fixed area defined the position of a linear slider. **(2)** Linear slider is used to manually compress the staple sample, and the slider is subsequently returned to its initial position so that the staple ensemble can later be expanded. **(3)** The rightmost embedded T shape is translated linearly, and the load cell records tensile forces

of entangled media behavior on prior loading via tensile experiments.

3 Entangled material characterization

3.1 Methods: material tensile test apparatus

To test the effects of initial loading on the strength of geometrically entangled materials, we construct a materials testing apparatus (see Fig. 7). The setup enables controlled compressive loading of a staple ensemble, as well as subsequent tensile stress on this ensemble. A single axis load cell (CALT DYLY 30 Kg S-Beam Load Cell) measures tensile forces during pulling, and linear motion is generated via a lead screw and stepper motor (Nema 23). We measure force-strain relationships of a staple ensemble (1 kg of material distributed across a 26 $\times$ 10.1 $\times$ 11.7 cm^3 open top box), for different initial conditions. Staples are originally scattered in a subset of the box and are manually compressed various distances (0, 1.25, 2.5, and 5 cm) to a final staple sample length of 18.9 cm. T-shapes, which are embedded in the box during staple scattering, are pulled apart via the lead screw assembly for a distance of 6.4 cm, and forces are recorded with the load cell and an amplifier chip (HX711) to an Arduino Uno. We perform three tests for

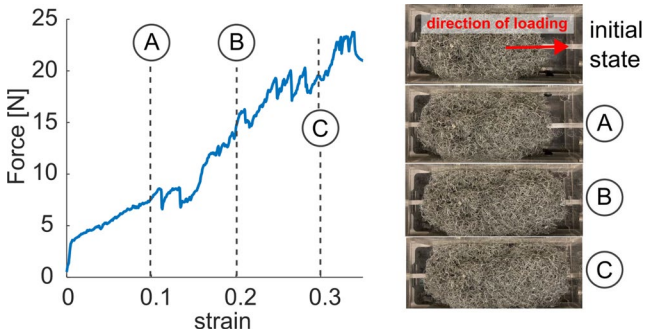

Fig. 8 Single trial tensile testing data. **(Left)** Sample force vs. strain relationship for a single trial of a staple ensemble with 10% initial compression. **(Right)** The corresponding photos of the staple ensemble at different strain values. Direction of loading during tensile testing experiments is indicated

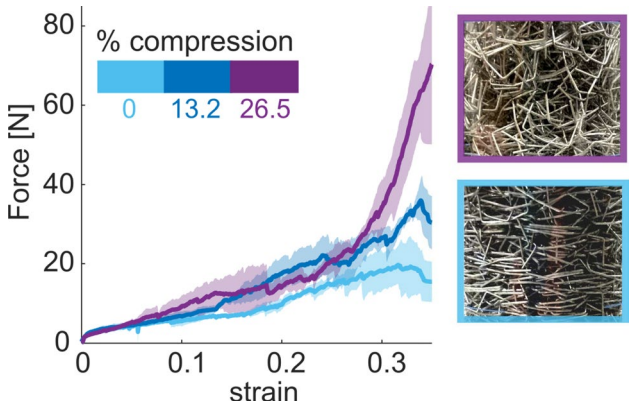

Fig. 9 Force-strain relations for staple samples with different initial compressions. Three different initial compressions are shown, with values indicated in the colorbar. Means and standard deviations over three trials are represented with solid lines and shaded regions, for each of the three compression values tested. **(Sidebar)** Two images of scattered (blue) and pushed (purple) material samples show that previously compressed staples are less likely to be geometrically aligned, and thus, are more entangled

each compression value, manually resetting and compressing the staples the desired distance before each tensile test. Note that in this apparatus, the staple ensemble is not pulled to full separation – in future experiments, measuring tensile forces during full extension may reveal further properties of these entangled materials.

3.2 Material testing results

For small initial compressions, tensile forces increase with strain but are locally non-monotonic (a trial at 10% compression is shown in Fig. 8). This trial includes local yield events which lead to momentary decreases in tensile force;

we hypothesize these events correspond to bending or breaking of entangled contacts between individual staples. Such "local yielding" events occurring during tensile loading have been observed in prior studies of entangled media behavior [24].

As shown in Fig. 9, for an uncompressed staple ensemble, the tensile force increases at a constant rate with strain, across all strain values tested. However, for staple ensembles which have been initially compressed (26.5% compression, for example), the force-strain relation has a slow initial rise, with a slope that increases markedly for strain >0.25. For strain less than ≈ 0.25, we observe comparable tensile forces across compression values, but as strain increases above this point, the behavior transitions and reveals the role of initial compression on tensile strength.

This behavior is further demonstrated in Fig. 10, which shows that larger initial compressions tend to increase tensile forces; however, this increase is more pronounced at higher values of strain. For example, at strain = 0.3, the 26.5%-compressed staple ensemble on average exerted 34.4 ± 7 N of tensile force, nearly double the 18.2 ± 4.9 N registered by the uncompressed sample. In contrast, at 0.1 strain, the 26%-compressed staple ensemble exerted 9.3 ± 2.7 N of tensile force, comparable to the 5.6 ± 1.3 N from the uncompressed sample. In other words, the role of initial compression on material strength is most apparent when the material has begun to separate while in tension.

These results demonstrate the complex rheological properties of entangled materials, as they respond differently depending on prior loading. In the robophysical experiments, the "pushed" material state has some initial compression (which likely varies throughout the material), while the "scattered" case has little to no initial compression. We posit that the behavior observed in our tensile tests points to the consistency observed in excavation of pellets during the "scattered" trials, in that tensile forces remain low across strain values (throughout the separation process). In contrast, if the "pushed" material is compressed during preparation, our results suggest that not only will the excavation process require more tearing force, but there will be greater variability in these forces, especially at high strain or once the material has been initially "stretched." As a result, our robotic platform may have been capable of initial material separation, but due to the entanglement elicited by initial compression, very large tensile forces were still present in the ensemble which led to occasional excavation failures in the "pushed" scenarios. We posit the frequent excavation failures observed during these trials may be attributed to this unusual compression-dependent strengthening of entangled materials.

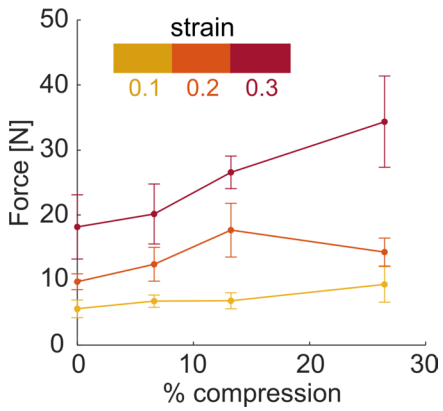

Fig. 10 Effect of initial compression on tensile force. Tensile force vs. various initial compression, for three different strain amounts, whose values are indicated in the colorbar. Error bars indicate standard deviation over three trials for each combination of strain and initial compression. The effect of initial compression on tensile strength is most evident at larger strain values

4 Conclusion & future work

We developed a robophysical platform capable of manipulating and transporting geometrically entangled media. This agent represents one of the first mobile platforms to successfully tear and manipulate highly cohesive media. We demonstrated that the robot can operate autonomously over several hours, basing decisions only on local environmental inputs. We also studied how robot performance was affected by the properties of the geometrically cohesive particles, and showed that preparation of entangled media significantly affected overall excavation performance.

We observed several unexpected behaviors in this work. For example, we observed that "pushing" of scattered U-shaped particles resulted in a *decrease* in volume fraction by 39% relative to the baseline "scattered" state. We also observed that previous compression of a staple ensemble resulted in up to a 108% increase in force required to tear the material. These results highlight that, in addition to packing density and particle shape [31–34], other aspects such as particle entanglement [26, 35, 36] and alignment [37–40] may be necessary to characterize the behavior of entangled granular media. Future work should expand upon the tensile testing trials performed here to inform more effective robotic excavation sequences and jaw geometries for known material properties.

Robotic teams capable of achieving complex construction tasks would be of value in engineering and science. For example, recent NASA missions such as the Artemis

project have targeted constructing bases on the moon and other planets [41, 42]. However, transporting external material to these locations is often too costly or prohibitive. Small mobile robots capable of building structures from lunar regolith or other found material could alleviate problems associated with material transport [43, 44]. Studies of lunar regolith samples have revealed complex particle shapes [45] with concavity [46], suggesting the potential viability of aleatory construction methods in extraterrestrial environments. Similarly, in remote or undeveloped locations on earth, robotic agents capable of constructing from resources in their local environments could reduce costs associated with construction equipment and shipping [47, 48] or assist in disaster response through rubble removal and reorganization [49]. Finally, given that diverse organisms [50–53] manipulate geometrically cohesive granular matter, insights from robophysical studies of robot swarms [54–56] can be used to develop hypotheses for collective biological construction.

Appendix A: Details of robophysical platform design and sensing strategy

The robot is equipped with a 5400 mAh 7.4 V LiPo battery, which directly powers the OpenCM9.04 microcontroller, and feeds into a Pololu Step-Up Voltage Regulator U3V70A set to 11.1 V for the motors. Under normal operation, to move forward or backward, the robot rotates its rear whegs. However, periodically, the system will instead use its limbs to propel itself forward in either a "crutch" or "sweep" maneuver. These maneuvers consist of a stride and swing phase (Fig. 11A) where the limb tip is in contact with the ground during the stride and is raised off the ground during swing. We use directionally compliant limbs, similar to that described in [57], to simplify the control needed for obstacle negotiation during the swing phase without impeding the thrust generated during the stride phase.

During the "crutch" motion, both limbs' roll motors are fixed to point outwards while the second motors rotate each limb 180°, which constitutes a stride motion. This results in the robot moving forward while pitching upwards and eventually landing back on its chassis. This maneuver serves to free the robot from any potential obstacles encountered during material transport. During the "sweep" motion, the motors on each limb are coordinated such that the stride length is maximized while the robot body maintains a fixed angle with respect to the ground. This maneuver provides less net propulsion than a crutch but it results in a less

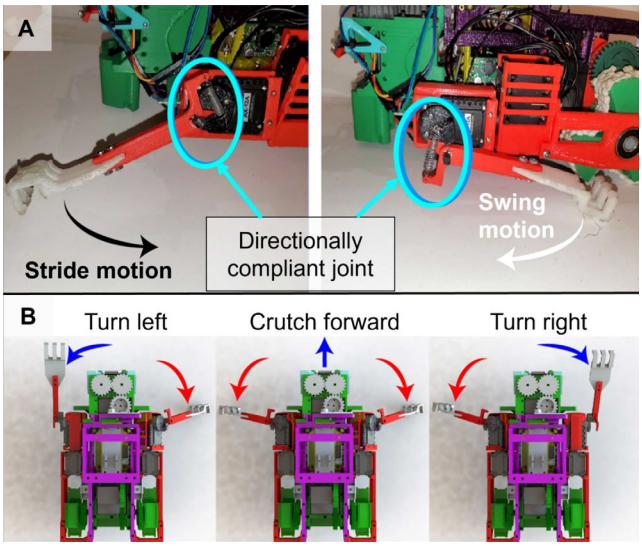

Fig. 11 Illustrations of robot locomotion strategies **A** View of the spring-loaded directionally compliant joint attached to the claw assembly. Both the stride (protraction) and swing (retraction) phases are illustrated. **B** Schematic of the robot arm motion in red and resultant turning motion in blue

substantial impact with the ground at the end of the motion, making it preferable while carrying material. To turn, the robot uses these same maneuvers but with only a single active limb (Fig. 11B). By choosing between maneuvers, the robot is able to effectively locomote in heterogeneous environments such as those created during transport of cohesive material.

Sensing modalities

The robot is equipped with a suite of sensors that receive environmental signals and guide subsequent behaviors. Both the Sparkfun ICM-20948 IMU and the Sparkfun VL6180 time-of-flight rangefinder are used to inform locomotion maneuvers. The rangefinder indicates when an obstacle is in front of the robot, which triggers a reversing motion. The IMU is used to indicate when body motion (specifically, pitching) is impeded, which in turn triggers a crutch maneuver. The Adafruit TCS34725 RGB color sensor enables the robot to react to fixed colored lights in its environment (such fixed environmental signals are used by other robotic swarm systems [58, 59]). Lastly, the robot is equipped with two systems to detect piles of previously deposited material that are independently operated by Dynamixel XL320 motors: the "antenna" and the 2-megapixel ArduCAM. The antenna uses the motor encoder to detect the height of piles 10 cm in front of the robot and serves as a form of short-range

sensing. The ArduCAM provides long-range sensing in the form of 320x240 monochrome images, which allows for basic vision methods that can detect piles over 10 cm in front of the robot. Overall, these sensors allow the agent to reliably locomote in obstacle laden scenarios and respond to environmental signals in the form of color or material deposits.

Appendix B: Details of robophysical platform experimental setup

To explore strategies for manipulating and transporting cohesive material, we construct an arena (length = 1.8 m, width = 1.2 m) with colored lights serving as environmental signals to guide the robot (Fig. 12A). The excavation and deposition areas are denoted with blue and red lights, respectively, and the arena is enclosed with blackout curtains to avoid outside interference. IR webcams provide an overhead view and a close-up view of the excavation area (Fig. 12B1 and B2). Each trial begins with an initial seed pile that the agent detects. The robot then deposits material over the next 2 hours, after which the trial ends and we weigh the total amount of material transported.

Appendix C: Details of robophysical platform finite state machine

The robotic agent is equipped with a finite state machine (FSM) (Fig. 13) based on the testing environment described in the prior section. The robot follows instructions encoded by the FSM, in order to excavate material, transport it to the deposition site, locate an existing deposit, and return to the excavation site to repeat the process. The transitions between behaviors are governed by environmental cues, which are detected by sensors as described in Section Appendix A. Turning is initiated after successful excavation or deposition and is only stopped once the RGB sensor detects a local maximum in the desired color value. Once the robot is moving towards the excavation site (blue), it will begin the excavation procedure until it detects that material has remained within its jaws.

While the robot is moving to deposit, it takes a picture using the ArduCAM and searches for a pile by counting the number of "dark" pixels (below a threshold) that exist in a column, for which two disconnected "bright" regions (maximum intensity) are also present. The robot then chooses the largest group of connected columns within an image. This method amounts to looking for the two LED strips that define the excavation site (the bright regions) and searching for shadows (dark pixels) that correspond to piles of staples (Fig. 12C). The robot then turns towards the largest group

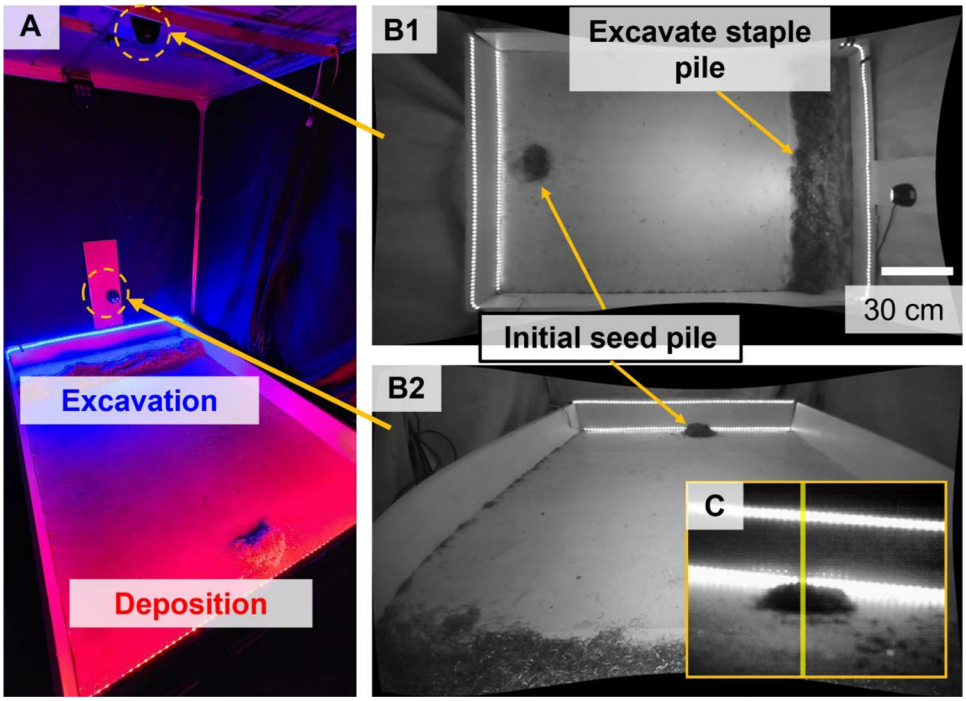

Fig. 12 **A** Side view of the testing arena with colored lights. The excavation site, with a staple pile covering its base, is lit with blue LEDs; the designated deposit wall is lit with red LEDs. The initial seed pile is situated along the deposit wall. **B1-2** Images from the ceiling and front night-vision camera. **C** Images taken by the ArduCAM which are used to detect existing piles

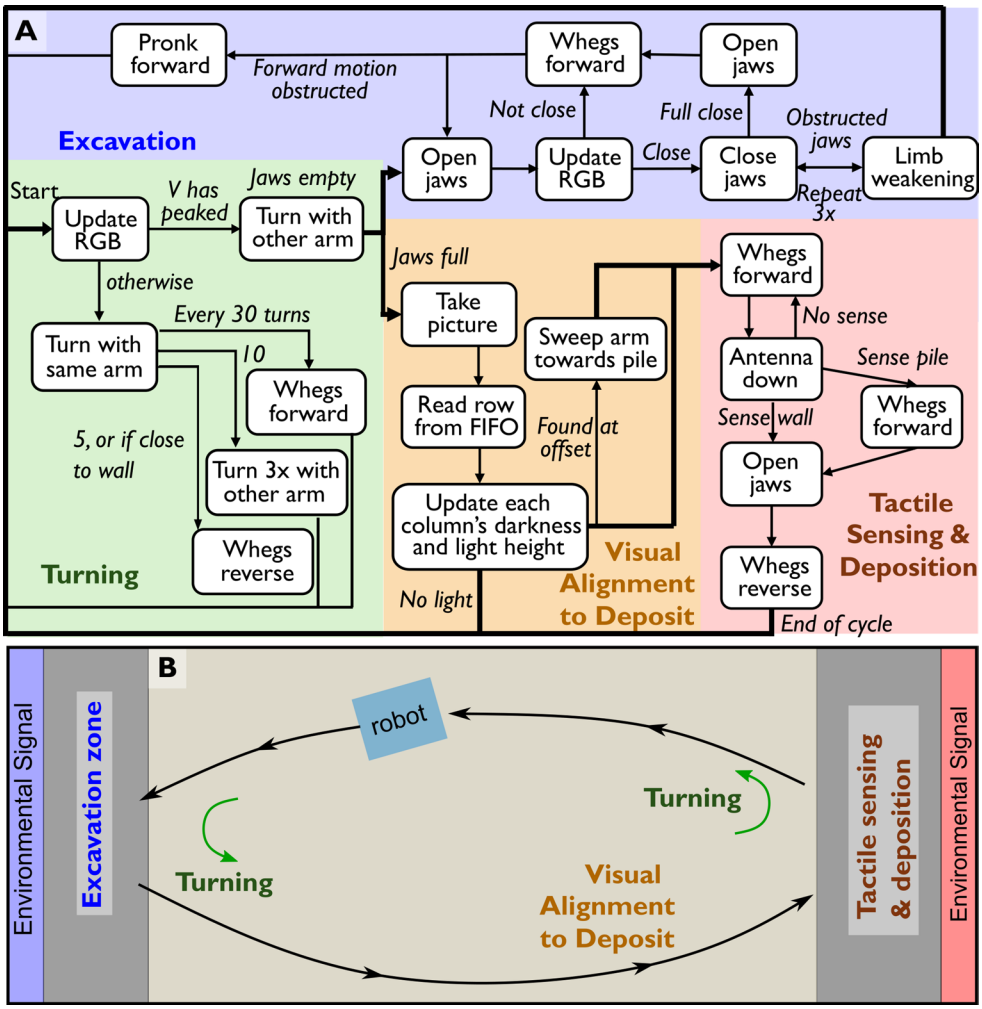

Fig. 13 **A** State machine diagram for excavation and deposit sequences. Different stages of operation are indicated with different colors. Bold lines indicate a transition in state between any of these four stages. **B** Visual representation of various robot states within its testing arena

and transitions to the final state of the FSM. Here, it will search with its antenna and deposit its material either at the existing pile or at the wall and then begin turning towards the excavation site, thus completing one cycle of material excavation and deposition.

Supplementary Information The online version contains supplementary material available at https://doi.org/10.1007/s10035-025-01597-6.

Acknowledgements L.T. was supported by NSF Grant #IOS-2019799. D.S. was supported by NSF Physics of Living Systems (PoLS) and the Office of the Executive Vice President for Research (EVPR). J.H. was supported by the Georgia Tech President's Undergraduate Research Award (PURA) program. We also thank the ARO MURI award no. W911NF-19-1-0233 for support throughout this research.

Author contributions DS, JH, and LT contributed to ideation, design, and control strategy of the robophysical model. DS designed and fabricated original robot prototypes. JH assisted with robotic construction and testing, and wrote autonomous control algorithms. LT assisted with robot mechanical design and testing in controlled material preparation states. LT designed and built the staple tensile testing apparatus and performed tensile testing experiments. DG and MG directed the high-level vision of the project and advised experimental protocols. LT, DS, and JH wrote sections of the manuscript. All authors contributed to manuscript revision, read, and approved the submitted version.

Data availability Data is provided within the manuscript or supplementary information files.

Declarations

Conflict of interest The authors declare no Conflict of interest.

References

1. Petersen, K.H., Napp, N., Stuart-Smith, R., Rus, D., Kovac, M.: A review of collective robotic construction. Sci. Robot. **4**(28), 8479 (2019). https://doi.org/10.1126/scirobotics.aau8479
2. Werfel, J., Petersen, K., Nagpal, R.: Designing collective behavior in a termite-inspired robot construction team. Science **343**(6172), 754–758 (2014). https://doi.org/10.1126/science.1245842
3. Seo, J., Yim, M., Kumar, V.: Assembly planning for planar structures of a brick wall pattern with rectangular modular robots. In: 2013 IEEE International Conference on Automation Science and Engineering (CASE), pp. 1016–1021 (2013). https://doi.org/10.1109/CoASE.2013.6653996
4. Napp, N., Nagpal, R.: Distributed amorphous ramp construction in unstructured environments. In: Distributed Autonomous Robotic Systems. Springer Tracts in Advanced Robotics, pp. 105–119 (2014). https://doi.org/10.1007/978-3-642-55146-8_8
5. Saboia, M., Thangavelu, V., Napp, N.: Autonomous multi-material construction with a heterogeneous robot team. Robot. Auton. Syst. **121**, 103239 (2019). https://doi.org/10.1016/j.robot.2019.07.009
6. Kristensen, E., Gramazio, F., Kohler, M., Langenberg, S.: Complex concrete constructions. In: Conference on Computer-Aided Architectural Design Research in Asia (CAADRIA 2013), vol. 613, pp. 622 (2013)
7. Silva, M.: Autonomous Adaptive Modification of Unstructured Environments. Ph.D. thesis, State University of New York at Buffalo (2019). https://www.proquest.com/docview/2320957977/abstract/4A8BA4DC04954E39PQ/1
8. Furrer, F., Wermelinger, M., Yoshida, H., Gramazio, F., Kohler, M., Siegwart, R., Hutter, M.: Autonomous robotic stone stacking with online next best object target pose planning. In: 2017 IEEE International Conference on Robotics and Automation (ICRA), pp. 2350–2356 (2017). https://doi.org/10.1109/ICRA.2017.7989272
9. Thangavelu, V., Liu, Y., Saboia, M., Napp, N.: Dry Stacking for Automated Construction with Irregular Objects. In: 2018 IEEE International Conference on Robotics and Automation (ICRA), pp. 4782–4789 (2018). https://doi.org/10.1109/ICRA.2018.8460562
10. Matl, C.C.: Interactive perception for robotic manipulation of liquids, grains, and doughs. PhD Thesis, University of California, Berkeley (2021)
11. Schenck, C., Tompson, J., Levine, S., Fox, D.: Learning robotic manipulation of granular media. In: Proceedings of the 1st Annual Conference on Robot Learning. Proceedings of Machine Learning Research, vol. 78, pp. 239–248 (2017)
12. Tuomainen, N., Blanco-Mulero, D., Kyrki, V.: Manipulation of granular materials by learning particle interactions. IEEE Robot. Autom. Lett. **7**(2), 5663–5670 (2022). https://doi.org/10.1109/LRA.2022.3158382
13. Keller, S., Jaeger, H.M.: Aleatory architectures. Granular Matter **18**, 1–11 (2016). https://doi.org/10.1007/s10035-016-0629-x
14. Murphy, K., Roth, L., Peterman, D., Jaeger, H.: Aleatory construction based on jamming: stability through self-confinement. Archit. Des. **87**(4), 74–81 (2017). https://doi.org/10.1002/ad.2198
15. Dierichs, K., Menges, A.: Towards an aggregate architecture: designed granular systems as programmable matter in architecture. Granul. Matter **18**(2), 25 (2016). https://doi.org/10.1007/s10035-016-0631-3
16. Dierichs, K., Menges, A.: Designing architectural materials: from granular form to functional granular material. Bioinspir. Biomimet. **16**(6), 065010 (2021). https://doi.org/10.1088/1748-3190/ac2987
17. Dierichs, K., Kyjánek, O., Loučka, M., Menges, A.: Construction robotics for designed granular materials: in situ construction with designed granular materials at full architectural scale using a cable-driven parallel robot. Construct. Robot. **3**(1), 41–52 (2019). https://doi.org/10.1007/s41693-019-00024-6
18. Aejmelaeus-Lindström, P., Willmann, J., Tibbits, S., Gramazio, F., Kohler, M.: Jammed architectural structures: towards large-scale reversible construction. Granul. Matter **18**(2), 28 (2016). https://doi.org/10.1007/s10035-016-0628-y
19. Aejmelaeus-Lindström, P., Rusenova, G., Mirjan, A., Medina Ibáñez, J., Gramazio, F., Kohler, M.: Rock print pavilion: robotically fabricating architecture from rock and string. Construct. Robot. **4**(1), 97–113 (2020). https://doi.org/10.1007/s41693-020-00027-8
20. Savoie, W., Tuazon, H., Tiwari, I., Bhamla, S.M., Goldman, D.I.: Amorphous entangled active matter. Soft Matter **19**(10), 1952–1965 (2023). https://doi.org/10.1039/D2SM01573K
21. Savoie, W., Berrueta, T., Jackson, Z., Pervan, A., Warkentin, R., Li, S., Murphey, T.D., Wiesenfeld, K., Goldman, D.I.: A robot made of robots: emergent transport and control of a smarticle ensemble. Science (2019). https://doi.org/10.1126/scirobotics.aax4316
22. Gravish, N., Franklin, S.V., Hu, D.L., Goldman, D.I.: Entangled granular media. Phys. Rev. Lett. **108**(20), 208001 (2012). https://doi.org/10.1103/PhysRevLett.108.208001
23. Gravish, N., I. Goldman, D.: Entangled granular media. In: Fluids, Colloids and Soft Materials, pp. 341–354 (2016). https://doi.org/10.1002/9781119220510.ch17
24. Franklin, S.: Extensional rheology of entangled granular materials. Europhys. Lett. **106**(5), 58004 (2014). https://doi.org/10.1209/0295-5075/106/58004
25. Sohn, Y., Pezeshki, S., Barthelat, F.: Tuning geometry in staple-like entangled particles: pick-up experiments and monte Carlo simulations. Granul. Matter **27**, 55 (2025). https://doi.org/10.1007/s10035-025-01531-w
26. Pezeshki, S., Sohn, Y., Fouquet, V., Barthelat, F.: Tunable entanglement and strength with engineered staple-like particles: experiments and discrete element models. J. Mech. Phys. Solids **200**, 106127 (2025). https://doi.org/10.1016/j.jmps.2025.106127
27. Karapiperis, K., Monfared, S., Macedo, R.B.D., Richardson, S., Andrade, J.E.: Stress transmission in entangled granular structures. Granul. Matter **24**(3), 91 (2022). https://doi.org/10.1007/s10035-022-01252-4
28. Marschall, T.A., Franklin, S.V., Teitel, S.: Compression- and shear-driven jamming of U-shaped particles in two dimensions. Granul. Matter **17**(1), 121–133 (2015). https://doi.org/10.1007/s10035-014-0540-2
29. Aguilar, J., Zhang, T., Qian, F., Kingsbury, M., McInroe, B., Mazouchova, N., Li, C., Maladen, R., Gong, C., Travers, M., et al.: A review on locomotion robophysics: the study of movement at the intersection of robotics, soft matter and dynamical systems. Rep. Prog. Phys. **79**(11), 110001 (2016). https://doi.org/10.1088/0034-4885/79/11/110001
30. Quinn, R.D., Offi, J.T., Kingsley, D.A., Ritzmann, R.E.: Improved mobility through abstracted biological principles. In: IEEE/RSJ International Conference on Intelligent Robots and Systems, vol. 3, pp. 2652–2657 (2002). https://doi.org/10.1109/IRDS.2002.1041670
31. Hidalgo, R., Kadau, D., Kanzaki, T., Herrmann, H.J.: Granular packings of cohesive elongated particles. Granul. Matter **14**(2), 191–196 (2012). https://doi.org/10.1007/s10035-011-0303-2
32. Wegner, S., Stannarius, R., Boese, A., Rose, G., Szabo, B., Somfai, E., Börzsönyi, T.: Effects of grain shape on packing and dilatancy of sheared granular materials. Soft Matter **10**(28), 5157–5167 (2014). https://doi.org/10.1039/C4SM00838C

33. Pena, A., Garcia-Rojo, R., Herrmann, H.J.: Influence of particle shape on sheared dense granular media. Granul. Matter **9**(3), 279–291 (2007). https://doi.org/10.1007/s10035-007-0038-2
34. Jaeger, H.M., Miskin, M.Z., Waitukaitis, S.R.: From nanoscale cohesion to macroscale entanglement: opportunities for designing granular aggregate behavior by tailoring grain shape and interactions. In: AIP Conference Proceedings, vol. 1542, pp. 3–6 (2013). https://doi.org/10.1063/1.4811858
35. Rezanejad, A., Mousa, M., Lorenz, C.D., Howard, M., Forte, A.E.: Programmable entanglement of granular mechanical metamaterials. Adv. Funct. Mater. (2025). https://doi.org/10.1002/adfm.202516484
36. Brown, E., Mitchell, K.A., Nasto, A., Athanassiadis, A., Jaeger, H.M.: Strain stiffening due to stretching of entangled particles in random packings of granular materials. Phys. Rev. E **111**(2), 025408 (2025). https://doi.org/10.1103/PhysRevE.111.025408
37. Börzsönyi, T., Szabó, B., Törös, G., Wegner, S., Török, J., Somfai, E., Bien, T., Stannarius, R.: Orientational order and alignment of elongated particles induced by shear. Phys. Rev. Lett. **108**(22), 228302 (2012). https://doi.org/10.1103/PhysRevLett.108.228302
38. Börzsönyi, T., Szabó, B., Wegner, S., Harth, K., Török, J., Somfai, E., Bien, T., Stannarius, R.: Shear-induced alignment and dynamics of elongated granular particles. Phys. Rev. E **86**(5), 051304 (2012). https://doi.org/10.1103/PhysRevE.86.051304
39. Pol, A., Artoni, R., Richard, P., Conceição, P.R.N., Gabrieli, F.: Kinematics and shear-induced alignment in confined granular flows of elongated particles. New J. Phys. **24**(7), 073018 (2022). https://doi.org/10.1088/1367-2630/ac7d6d
40. Wegner, S., Börzsönyi, T., Bien, T., Rose, G., Stannarius, R.: Alignment and dynamics of elongated cylinders under shear. Soft Matter **8**(42), 10950–10958 (2012). https://doi.org/10.1039/C2SM26452H
41. Ehrenfried, M.: The Artemis Lunar Program Overview. In: The Artemis Lunar Program: Returning People To the Moon, pp. 7–47 (2020). https://doi.org/10.1007/978-3-030-38513-2_2
42. Khoshnevis, B.: Automated construction by contour crafting–related robotics and information technologies. Autom. Constr. **13**(1), 5–19 (2004). https://doi.org/10.1016/j.autcon.2003.08.012
43. Rossi, M., Sumini, V., Zanelli, A., Viscuso, S.: Computational design of an extreme livable lightweight environment on mars. J. Archit. Eng. **30**(2), 04024009 (2024). https://doi.org/10.1061/JAEIED.AEENG-1632
44. Mueller, R.P.: Construction with regolith. In: The Technology and Future of In-Situ Resource Utilization (ISRU): A Capstone Graduate Seminar (2017)
45. Tsuchiyama, A., Sakurama, T., Nakano, T., Uesugi, K., Ohtake, M., Matsushima, T., Terakado, K., Galimov, E.M.: Three-dimensional shape distribution of lunar regolith particles collected by the apollo and luna programs. Earth Planets Space **74**(1), 172 (2022). https://doi.org/10.1186/s40623-022-01737-9
46. Deitrick, S., Cannon, K.: Characterizing detailed grain shape and size distribution properties of lunar regolith. In: 53rd Lunar and Planetary Science Conference (2022)
47. Gerling, V., Von Mammen, S.: Robotics for Self-Organised Construction. In: 2016 IEEE 1st International Workshops on Foundations and Applications of Self* Systems (FAS*W), pp. 162–167 (2016). https://doi.org/10.1109/FAS-W.2016.45
48. Pradhananga, P., ElZomor, M., Santi Kasabdji, G.: Identifying the challenges to adopting robotics in the US construction industry. J. Constr. Eng. Manag. **147**(5), 05021003 (2021). https://doi.org/10.1061/(ASCE)CO.1943-7862.0002007
49. Gregory, J., Fink, J., Stump, E., Twigg, J., Rogers, J., Baran, D., Fung, N., Young, S.: Application of Multi-Robot Systems to Disaster-Relief Scenarios with Limited Communication. In: Field and Service Robotics: Results of the 10th International Conference, pp. 639–653 (2016). https://doi.org/10.1007/978-3-319-27702-8_42
50. Hansell, M.H.: Animal Architecture. Oxford University Press (2005)
51. Tschinkel, W.R.: The Fire Ants. Harvard University Press (2013)
52. Larsen, A., Larsen, J.R., Lane, S.N.: Dam builders and their works: beaver influences on the structure and function of river corridor hydrology, geomorphology, biogeochemistry and ecosystems. Earth Sci. Rev. **218**, 103623 (2021). https://doi.org/10.1016/j.earscirev.2021.103623
53. Andrade-Silva, I., Godefroy, T., Pouliquen, O., Marthelot, J.: Cohesion of bird nests. In: EPJ Web of Conferences, vol. 249, p. 06014 (2021). https://doi.org/10.1051/epjconf/202124906014
54. Aguilar, J., Monaenkova, D., Linevich, V., Savoie, W., Dutta, B., Kuan, H.-S., Betterton, M.D., Goodisman, M.A.D., Goldman, D.I.: Collective clog control: Optimizing traffic flow in confined biological and robophysical excavation. Science **361**(6403), 672–677 (2018). https://doi.org/10.1126/science.aan3891
55. Aina, K.O., Avinery, R., Kuan, H.-S., Betterton, M.D., Goodisman, M.A.D., Goldman, D.I.: Toward task capable active matter: learning to avoid clogging in confined collectives via collisions. Front. Phys. **10**, 735667 (2022). https://doi.org/10.3389/fphy.2022.735667
56. Carey, N.E., Bardunias, P., Nagpal, R., Werfel, J.: Validating a termite-inspired construction coordination mechanism using an autonomous robot. Front. Robot. AI (2021). https://doi.org/10.3389/frobt.2021.645728
57. Ozkan-Aydin, Y., Chong, B., Aydin, E., Goldman, D.I.: A systematic approach to creating terrain-capable hybrid soft/hard myriapod robots. In: 2020 3rd IEEE International Conference on Soft Robotics (RoboSoft), pp. 156–163 (2020). https://doi.org/10.1109/RoboSoft48309.2020.9116022
58. Garnier, S., Tache, F., Combe, M., Grimal, A., Theraulaz, G.: Alice in pheromone land: An experimental setup for the study of ant-like robots. In: 2007 IEEE Swarm Intelligence Symposium, pp. 37–44 (2007). https://doi.org/10.1109/SIS.2007.368024
59. Arvin, F., Krajník, T., Turgut, A.E., Yue, S.: Cosϕ: Artificial pheromone system for robotic swarms research. In: 2015 IEEE/RSJ International Conference on Intelligent Robots and Systems (IROS), pp. 407–412 (2015). https://doi.org/10.1109/IROS.2015.7353405